AIAA JOURNAL
Vol. 34, No. 6, June 1996

Three-Dimensional Wake Formations Behind a Family of Regular Polygonal Plates

H. Higuchi,* R. W. Anderson,† and J. Zhang‡
Syracuse University, Syracuse, New York, 13244-1240

The experiments were conducted in water to study the initial wake formations behind various polygonal plates placed normal to the starting flow. The models included triangular, square, hexagonal, and octagonal plates. Because of nonuniform self-induced velocity, the initial vortex structure behind each polygonal plate was arched in the axial direction, and pairs of counter-rotating longitudinal vortices induced inward motion of the vortex structure at each corner. The evolution of free polygonal vortex loops was numerically simulated using a simplified three-dimensional vortex segment method to demonstrate the mechanism for the observed vortex deformation.

Nomenclature

A_p	= acceleration parameter, $D_{eq}a/U_0^2$
a	= acceleration, dU/dt
D	= side length of square plate
D_{eq}	= equivalent disk diameter
Re	= steady-state Reynolds number, U_0D_{eq}/v
Re_c	= acceleration Reynolds number, $\sqrt{(D_{eq}^3a)}/v$
T	= nondimensional time, U_0t/D_{eq}
t	= time
t_c	= time scale, $\sqrt{(D_{eq}/a)}$
U	= freestream velocity
U_0	= steady freestream velocity
X	= axial distance
v	= kinematic viscosity

Introduction

THE initial stage of wake formation behind a normal two-dimensional flat plate has been studied fairly extensively (e.g., see Refs. 1 and 2 and references cited therein). On the other hand, the wake formations behind axisymmetric and three-dimensional bluff bodies in starting flows have been investigated to a lesser degree. In an earlier experiment on the wake behind a circular disk,[3,4] the vortex ring that formed in the wake subsequently underwent Widnall-type instability and nonplanar deformations. After the largely distorted vortex was shed, a steady-state wake structure (though naturally three dimensional and unsteady) was reached.

Instability of the isolated vortex ring has received significant attention since Widnall et al.[5] published their inviscid theory; recent contributions include a finite difference calculation by Shariff et al.[6] Studies on free shear flows with nonaxisymmetric cross sections have been conducted with jets issuing from noncircular orifices. A faster mixing process and axis switching as a result of the longitudinal vortices have been observed in the near field of a square jet.[7] Similar vortex interactions are expected in the wake flow, though no systematic study exists to the authors' knowledge.

Freymuth et al.[8] visualized the starting vortex systems behind low-aspect-ratio wings at a high angle of attack. At the leading edges of square, rectangular, and delta wings, an arching vortex was clearly identified. The very early stage of the starting flow past a normal square plate was numerically simulated by Chua[9] using a three-dimensional vortex method by approximating the wall layer by closed vortex loops. Little or no vortex roll-up occurred at the corner, which was attributed to strong stretching of the vorticity at the corner.

The simulation by Chua and our observation behind a circular disk motivated a new set of experiments on bluff bodies placed normal to the starting flow. To study the three-dimensional wake formation, intrinsically three-dimensional geometry was selected. Equilateral polygons with sharp corners ranging from a triangular plate to an octagonal plate were tested. The hexagon and octagon were chosen as means of studying the effect of circumferential variation from the disk on the wake.

Experimental Setup

Test Facility

The experiments were conducted in a low-speed water channel at Syracuse University (Fig. 1). The test section was 0.61 m in both width and height and 2.44 m in length. A free surface boundary existed at the top. A window is incorporated at the end of the diffuser section to allow end views without disturbing the flowfield. The test section walls and end window were made of clear plastic.

The freestream velocity was controllable either by computer-generated voltage to the pump motor controller or by manual operation of the speed-control potentiometer. The fastest acceleration from rest was governed mainly by the inertia of the water, and as shown in Fig. 2, the freestream velocity time history under rapid manual control was highly repeatable for a given velocity setting. This mode was used in the present experiments. (Attention was paid so that the free-surface water level in the test section was level with the contraction section; otherwise minor flow velocity oscillations resulted during the startup.) Figure 2 shows the velocity time histories for two velocity settings used in the present experiment, and the observations were made during their initial accelerating flow regimes. The freestream velocity was monitored upstream of the model by a TSI fiber-optic laser Doppler velocimetry system that incorporated a frequency shifting. The hydrogen bubble wire placed upstream of the model or in the test area without the model indicated that the flow acceleration was uniform and devoid of any swirl to affect the present test.

The time after the flow startup may be normalized in various ways. For a flow impulsively started to a steady speed, the acceleration parameter A_p and the nondimensional time T as defined in the Nomenclature are suitable, whereas the process in the acceleration phase itself should be normalized by the acceleration alone as $t/t_c = t/[D_{eq}/(du/dt)]^{0.5}$. Finally, the distance traveled by the model normalized by the model dimension may be used in general starting flows. In the present paper, the time was left dimensional due to nonlinearity of acceleration; the various time scales and parameters are listed in Table 1. Note that the Reynolds number

Received May 3, 1995; revision received Feb. 2, 1996; accepted for publication Feb. 23, 1996.

*Professor, Department of Mechanical, Aerospace, and Manufacturing Engineering; currently Visiting Research Scientist, Institute of Space and Astronautical Science, 3-1-1 Yoshinodai, Sagamihara 229, Japan. Associate Fellow AIAA.

†Undergraduate Fellow, National Science Foundation Research Experiences for Undergraduates Program, Department of Mechanical, Aerospace, and Manufacturing Engineering; currently Graduate Student, Department of Mechanical and Aerospace Engineering, Princeton University, Princeton, NJ 08544.

‡Graduate Student, Department of Mechanical, Aerospace, and Manufacturing Engineering.

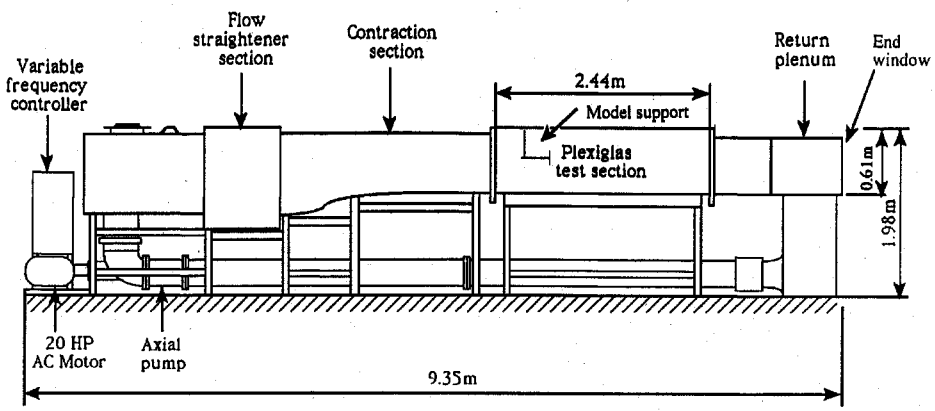

Fig. 1 Water channel.

Table 1 Model parameters

	Triangle	Square	Hexagon	Octagon
D_{eq}, cm	4.36	5.73	5.33	5.22
t_c, s	1.99	2.28	1.66	1.64
Re_c	954	1440	1710	1660
A_p	0.129	0.169	0.165	0.161
Re	2660	3500	4210	4120
U_0, cm/s	6.1	6.1	7.9	7.9

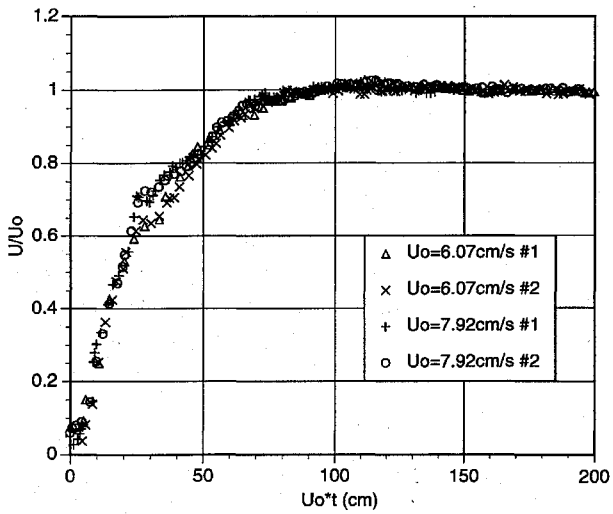

Fig. 2 Freestream velocity time history.

Re_c is defined by the acceleration rate, and a line fit to the initial acceleration phase ($U_0 t < 20$ cm) was used for the values presented to characterize the initial wake development.

Models and Flow Visualization Technique

The following equilateral polygonal geometries were chosen for the experiment: a triangle, a square, a hexagon, and an octagon. The individual polygonal models consisted of a dual 0.8-mm-thick plate separated by a 0.5-mm gap to allow the release of dye from the model edges. The fluorescein dye was gravity fed through a cantilever support (3.2-mm diameter) at the model centerline attached to a streamlined strut upstream. The strut was placed sufficiently far upstream (typically 300 mm) to minimize the disturbance to the wake; furthermore, the phenomena presented herein were observed before any disturbance convected from the strut reached the model. The density of the dye mixture closely matched that of the water.

To define a model size applicable to various geometries, an equivalent disk diameter having the same surface area was calculated for each model as listed in Table 1. For example, an equilateral triangle has an equivalent disk diameter that is 0.743 times its side length.

The fluorescent dye released in the wake was illuminated from above by an ultraviolet light. As the uniform illumination tended to mask the interior structure of the wake, additional laser light sheets were used. An illumination parallel to the model was placed 3.5 cm downstream of the model as needed and viewed through the end window of the channel. Laser sheets parallel to the flow were also used. The dye was injected at a fixed upstream location, and regardless of the type of illumination, the resulting streaklines carry integrated time history and need to be interpreted with caution.[10–12] The hydrogen bubble technique was used as a supplement; the hydrogen bubble wire can be placed at different positions in the flow, and the supply voltage can be pulsed to provide qualitative information on local velocity field. All of the flow visualizations were recorded with a Hi8 camcorder. The video tapes were then digitized at 30 frames per second for analysis and for reproduction. The flow visualizations were repeated several times, and the results were repeatable as to the geometry of the wake structure as well as its position, even though they may vary in their image quality. A similar flow visualization study was conducted in a towing tank, and the repeatability of the visualized flow may be quantitatively assessed in the report in terms of the vortex trajectories behind a disk.[3] The results reproduced in this paper are those with fluorescent dye.

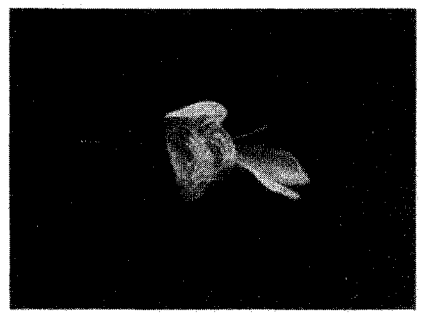

a) $t = 2.5$ s

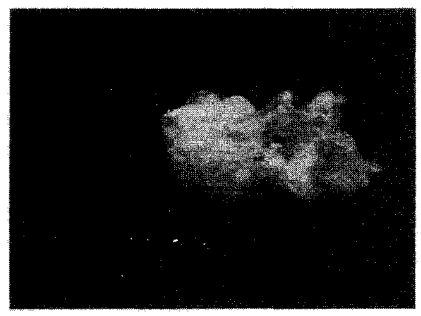

b) $t = 7.0$ s

Fig. 3 Wake development behind triangular plate: oblique view.

Results of Experiment

Triangular Plate

The results of the dye flow visualization in oblique view are shown in Figs. 3a and 3b. At an early stage of development (Fig. 3a), the individual vortex roll-up from each triangle edge takes place nonuniformly along its vortex axis. Deformation or arching of the

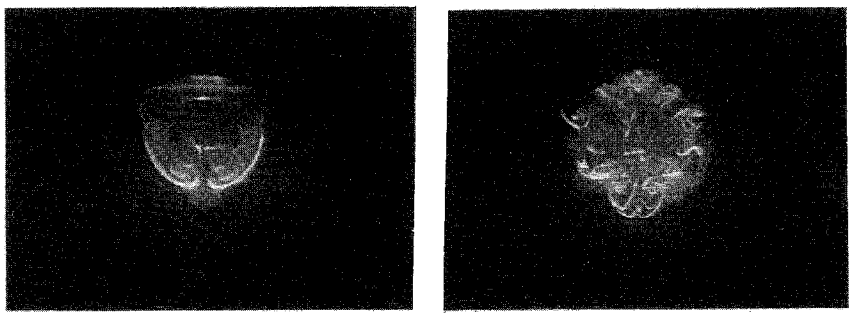

a) $t = 2.5$ s

c) $t = 4.5$ s

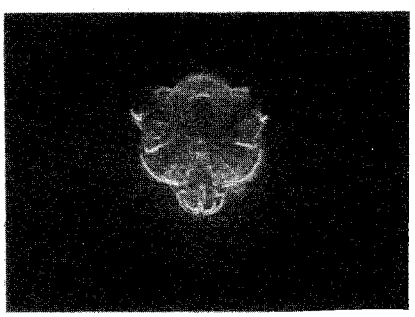

b) $t = 3.5$ s

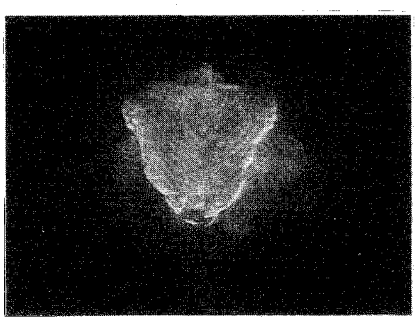

d) $t = 7.0$ s

Fig. 4 Wake development behind triangular plate: end view (uniform and cross-sectional illumination).

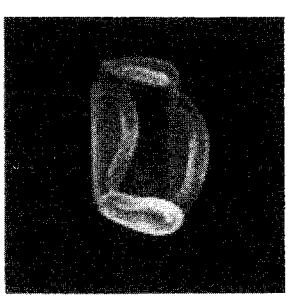

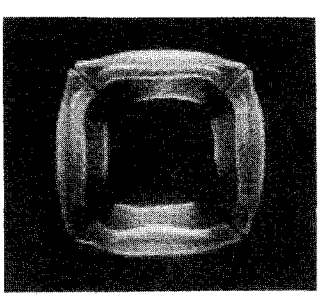

a) $t = 1.5$ s

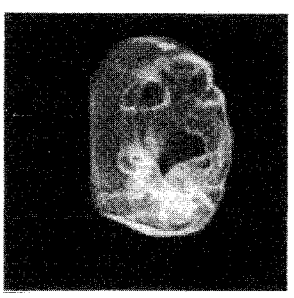

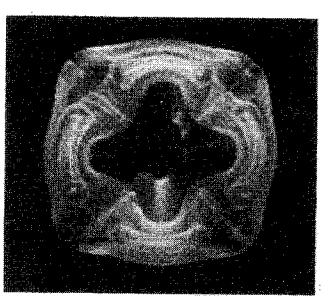

d) $t = 3.0$ s

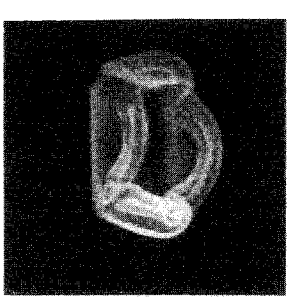

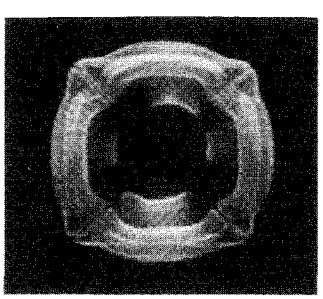

b) $t = 2.0$ s

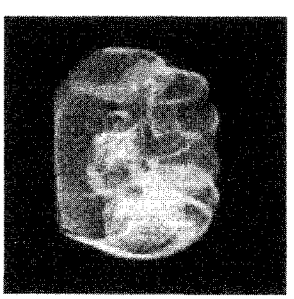

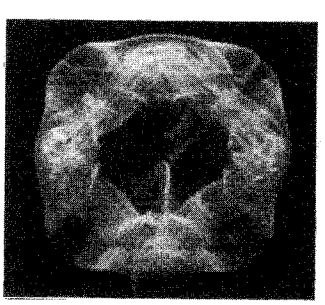

e) $t = 4.0$ s

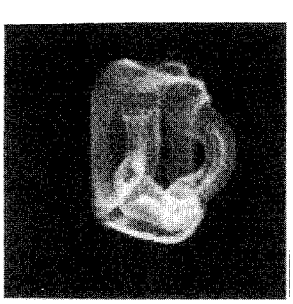

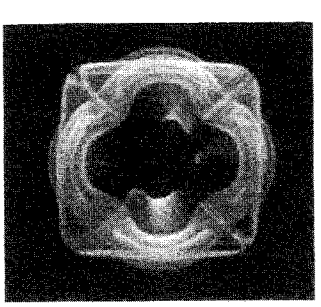

c) $t = 2.5$ s

Oblique view End view

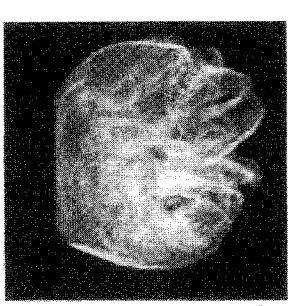

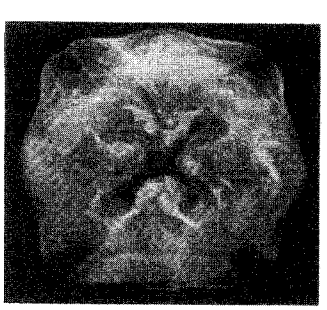

f) $t = 6.0$ s

Oblique view End view

Fig. 5a–f Wake development behind square plate.

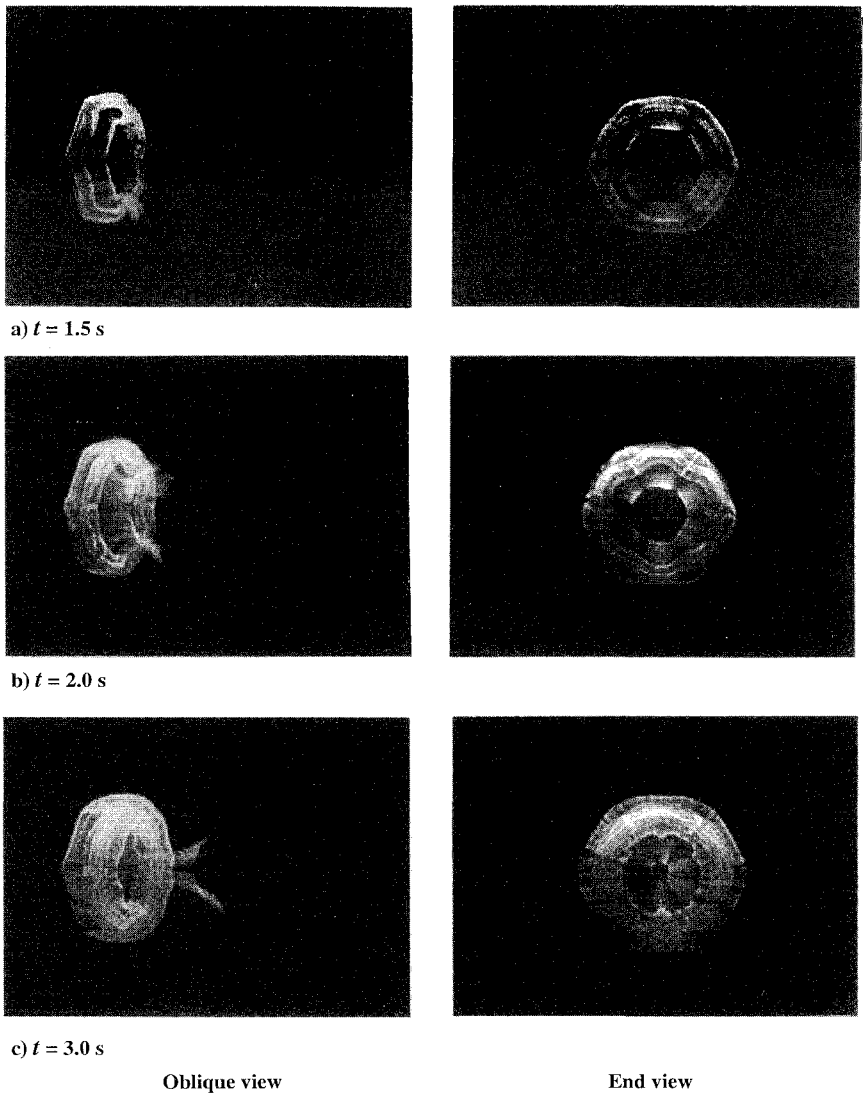

Fig. 6a–c Wake development behind hexagonal plate.

vortex tube can be seen in the figure. (The tail downstream is an artifact because of prematurely released dye. No editing or enhancement was used in the images in the paper.) Note that the vortex tubes near the corners are almost perpendicular to the rear face of the plate. These vortex tubes elongated downstream to form three hairpin vortices. Figure 3b shows a much later stage at which three vortices started to interact with each other. Further details of the process can be seen in end views given in Figs. 4a–4d. In addition to the uniform ultraviolet lighting, the laser sheet was projected from below, illuminating the plane 0.8 equivalent diameter downstream. Figure 4a shows three arched (hairpin) vortices crossing the plane of the laser sheet. At the corners of the triangle, the self-induced velocity of the arched vortices deforms the vortex structure away from the corners. The secondary hairpin vortex forms from the separated shear layer at each of three corners and the direction of rotation is opposite to the primary vortices. The formation of secondary vortices is shown in Fig. 4b. Three primary hairpin vortices as well as the secondary vortices stretch downstream (Fig. 4c) and start to interact with each other, eventually forming a completely three-dimensional wake. The laser sheet parallel to the plate in the near wake shows a clear triangular contour indicating a smooth parallel shear layer leaving each edge of the triangle (compare Figs. 4d and 3b). Further downstream, by contrast, the wake interface retained little of the original contour, with a high level of convolution even after the steady-state flow is reached.

Square Plate

For the square plate wake, care was taken to synchronize the dye release and the flow start. Two sequences of the flow development obtained from two camera angles are shown side by side as an oblique view and an end view in Fig 5. By $t = 1.5$ s, deformation of the initial vortex structure is apparent (Fig. 5a). The oblique view shows that this deformation is three dimensional in nature, with the vortex bowing in a streamwise direction along each side of the plate. This is the action that leads to streamwise vorticity, which in turn causes the deformation apparent in the end view. This deformation progresses throughout the first stage as a result of the counter-rotating vorticity components near four corners, resulting in a characteristic diamond shape towards the end of the sequence (see Figs. 5c–5e). By $t = 6$ s, in the last frame reproduced in Fig. 5f, a complex yet highly ordered and symmetric wake structure is revealed. Tongue-shaped structures have developed from four sides toward the center along the rear face of the model. This phenomenon is followed by the onset of instabilities, characterized by rapid vortex structure breakdown. A steady-state turbulent wake was established shortly afterward.

In an additional visualization experiment, a laser sheet perpendicular to the square plate was placed diagonally across the model. Initial flow direction from the vertex was along the rear surface toward the center of the plate. On the other hand, a laser sheet crossing the midpoints of the opposite sides showed that the flow separated past the side edges in a primarily streamwise direction shortly after the flow startup, resulting in distinct vortex formation. These observations were consistent with the results of the oblique and end views shown earlier. The same model was also subjected to a rapid linear acceleration and a sharp transition to the constant speed in a water towing tank, which was described elsewhere.[3] The overall flow patterns were the same, except for a much faster growth of the

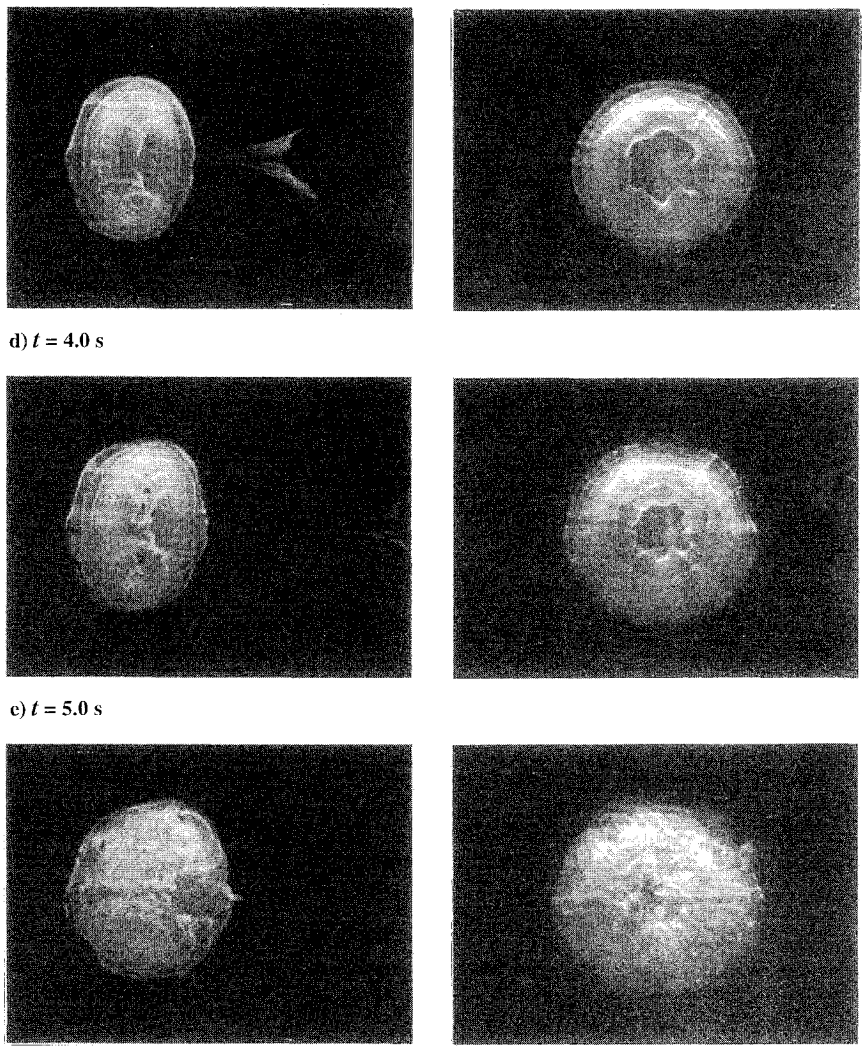

Fig. 6d–f Wake development behind hexagonal plate.

wake. The time history of the vortex position will be considered later in the discussion.

Hexagonal Plate

Oblique and end views of the wake behind the equilateral hexagonal plate were captured simultaneously using two cameras as shown in Fig 6. At $t = 1.5$ s, an arched vortex formed along each edge. A continuous but nonplanar vortex ring is seen in the oblique view at $t = 2$ s. The end view at the same time shows that the apex of the vortex ring has moved by 30 deg and now appears behind the flat edge of the model (Fig. 6b). Shortly afterward, the nonuniformly induced velocity brings the apex back into alignment with the corners of the hexagon, as shown in the end view at $t = 3$ s. The oblique view shows the dye trailing behind near the centerline of the wake. The dye-carrying fluid was entrained upstream by the vortex ring but encountered folding of streamlines to be detrained downstream. This phenomenon was more prominent in the visualization presented in an earlier paper on the experiment[10] and will be discussed further. In the end view at $t = 5$ s (Fig. 6e), multiple hexagonal patterns at different orientations can be seen. Flow symmetry starts to be lost by $t = 7$ s (corresponding to Fig. 6f), and later the end view video showed a pair of counter-rotating vortex motions that triggered the fully three-dimensional flow structure.

Octagonal Plate

The development of the wake behind the octagonal plate is shown in a sequence of oblique views in Fig. 7. The general evolution of the wake structure was relatively similar to that behind the hexagonal model and to that behind the disk.[3] At the beginning, shear layers rolled up from individual edges, and shortly afterwards a continuous but arched vortex ring was formed. In this sequence, a slightly premature release of dye caused an artifact at the upper half. In the earlier visualization, eight individual tails formed and elongated in a streamwise direction.[13] The formation of the tail structure will be addressed later. After $t = 7$ s, the wake became fully convoluted and three dimensional.

Discussion of Results

Vortex Method Simulation

The nonuniform nature of the induced velocity as a result of the polygonal free vortex ring can be inferred from the Biot–Savart law. Deformations and switchings of noncircular smoke rings were seen in an experiment by Toyoda and Hussain.[14] Similar deformation took place in the present wake flow. To gain further insight into the deformation process of the polygonal vortex structure, a simple numerical simulation was implemented using a three-dimensional vortex method after Chorin.[15] Only the free deformation and induced motion of a polygonal vortex loop under its own influence were simulated, and the presence of the model wall was ignored. The vortex loop was replaced by a finite number of straight vortex segments attached to each other. The vorticity is assumed to be concentrated at the midpoint of each segment, but each segment is given a finite core. The position of each control point is then updated because of local convection, and the core radius is adjusted to preserve

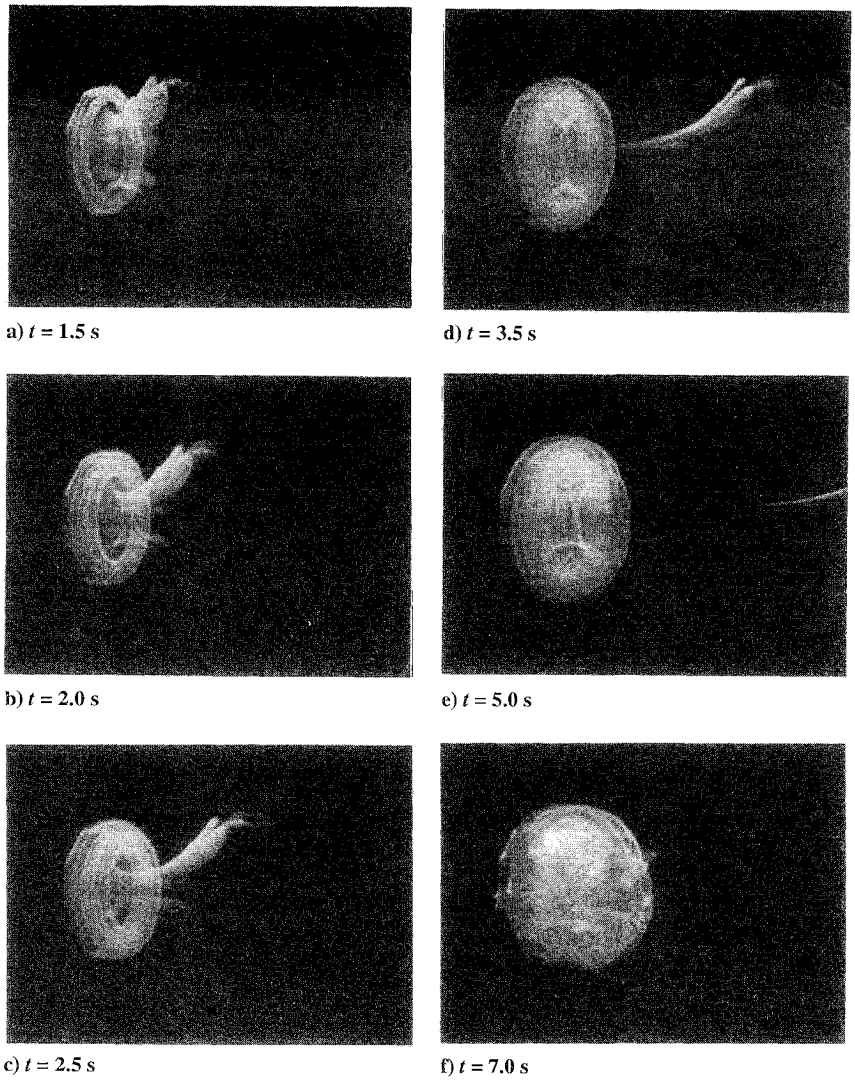

Fig. 7 Wake development behind octagonal plate.

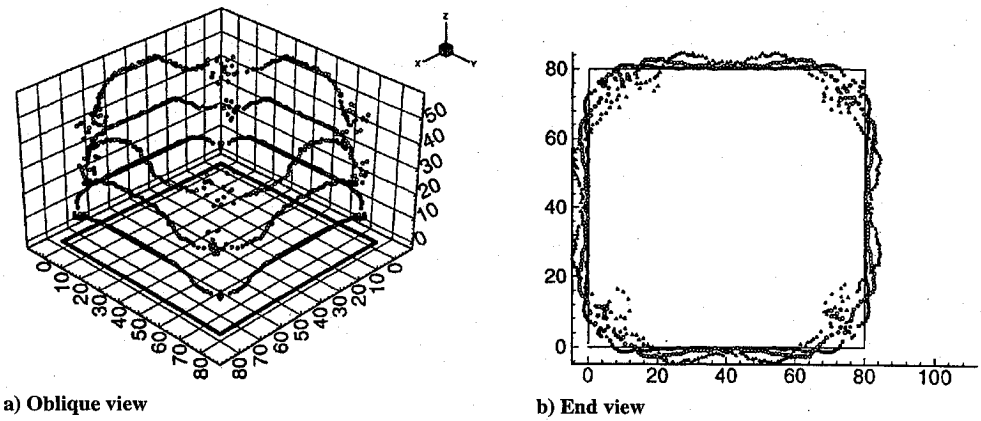

Fig. 8 Vortex segment method simulation of square vortex: ——, initial; ◇, $t = t_1$; ○, $T = 2t_1$; and ▲, $T = 3t_1$.

circulation in each segment. In the method implemented here, the number of segments is fixed at a sufficiently large number (300 minimum), and excessive stretching of any one segment that would necessitate additional resegmentation is assumed to be absent.

The numerical results for a square vortex loop are shown in Figs. 8a and 8b. (The value of the nondimensional time t_1 depends on such parameters as the nondimensional circulation but is not critical for the present comparison since the progression of the phenomena is nearly independent of these values.) The oblique view in Fig. 8a shows the arching of the vortex loop with time. The end view in Fig. 8b depicts the inward movement of the vortex loop at four corners as observed experimentally. Increased scatter of vortex segments at the corner may indicate some local crossings of vortex loops; thus the later computations are not shown. Figures 9a and 9b show a simulation of a hexagonal vortex loop. Again the magnitude of t_1 is not shown in the present illustration. Unlike the simulation of the square vortex loop with the same circulation, the amount of the arching of the vortex loop increases with time only up to a point. (Compare Figs. 8 and 9 at $T = 3t_1$, for example.) The end view in Fig. 9b shows a deformation of vortex loop with its apex out of

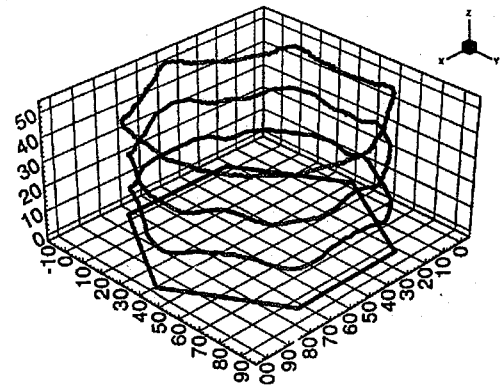

a) Oblique view

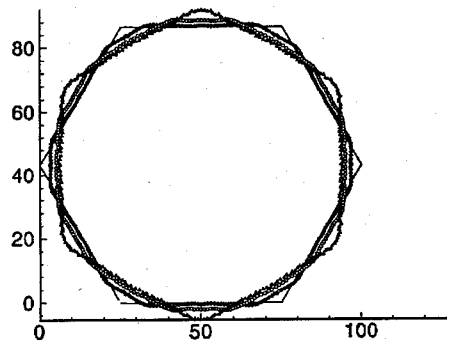

b) End view

Fig. 9 Vortex segment method simulation of hexagonal vortex: ——, initial; ◇, $t = t_1$; ○, $T = 2t_1$; and ▲, $T = 3t_1$.

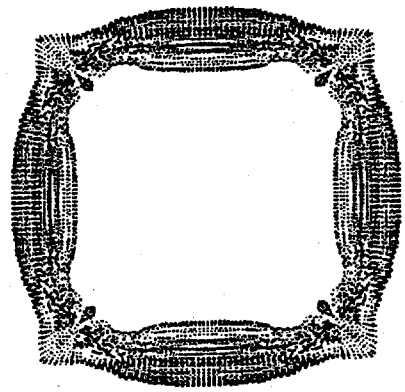

Front view

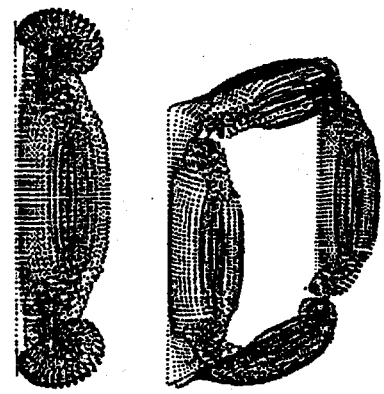

Side view Oblique view

Fig. 10 Three-dimensional vortex simulation of the impulsively started flow past a square plate, $U_0t/D = 0.4$ (Ref. 9).

phase with the hexagon corners. This displacement of the apex is in agreement with the flow visualization (see Fig. 6b, for example).

Naturally, the full extent of the complex flow phenomena observed in the present experiment cannot be expected to be analyzed in this simple simulation. Shariff et al.[6] solved the Navier–Stokes equations by the finite difference scheme to simulate the three-dimensional instability of vortex rings subjected to perturbations. Chua's numerical simulation,[9] however, is most closely related to the present experiment. He applied the three-dimensional vortex method to the wake behind a square plate, and the flow pattern compares well with the present flow visualization in the early stages as shown in Fig. 10. Corresponding nondimensional times were different; the difference, however, is partly attributable to the non-impulsive starting of flow in the present experiment. The vortex position on the meridian plane was compared with the present data in Fig. 11. The final freestream velocity was used for normalization, even though the water tunnel experiment shown here took place during the acceleration phase. As expected, data from rapid acceleration agree better with the impulsively started flow simulation. Even when plotted against the distance traveled, three sets of data did not produce a single curve. Pathlines emanating from the model vertex and those from the side edges also agreed well between the simulation and the present experiment. Because of a difficulty in Chua's computation, the results for later times are not available for comparison.

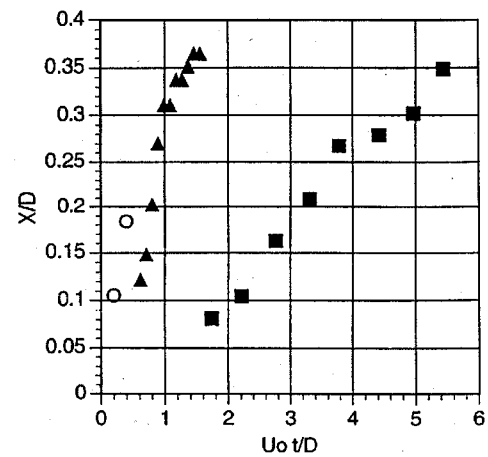

Fig. 11 Vortex position in the meridian plane behind a square plate: ▲, experiment: $A_p = 1.43$; ■, experiment: $A_p = 0.69$; and ○, computation-Chua: $A_p = \infty$.

Formation of Tail-Like Structures

The pulsed hydrogen bubble study was conducted in selected cases. Results indicated that the velocity outside the wake boundary was greater than that of the freestream and that it generated azimuthal vorticity in the recirculating region in a direction opposite to that of the vortex ring. When the dye was introduced into the potential flow region beyond the wake formation region, the induced velocity as a result of this azimuthal vorticity produced a well-structured pattern of dye. When the dye was present near the model edges before the flow startup, the dye filament was first stretched toward the model center along its rear face until the flow separated and formed a vortex. This velocity field caused the dye to form a tail. This process is illustrated in Fig. 3a behind the triangular plate, in Figs. 6a–6c behind the hexagonal plate, and in Figs. 7a–7d in the octagonal plate. In the earlier examples,[13] a prominent structure appeared when more dye was released before the flow startup. Similar patterns have been observed and numerically simulated behind a flat plate.[2] Behind a circular disk, axisymmetric lobe-like structures have been observed[3,4]; they appear to have been caused by the dye fluid marking the Kelvin–Helmholtz instability waves. The experiment and the axisymmetric vortex method simulation also compared well with regard to these flow structures.[16]

Subsequent tail formations were specific to the individual geometries. For example, behind the hexagonal plate six tails formed and became elongated (Fig. 5).Their azimuthal positions corresponded

to the corners of the equilateral polygon. A nonuniform but organized azimuthal vorticity field appeared to take effect. Shariff et al.'s computation[6] of a vortex ring subjected to perturbations showed a distinct nodal structure of azimuthal vorticity. As shown in the present flow visualizations, the three-dimensional streaks became visible as dye-carrying fluid was transported beyond the recirculating wake region. However, study of the video indicated that there was no longitudinal motion among or within these tail structures. This lack of rotation contrasts with the clear longitudinal vortices observed in the near field of the wake (e.g., see Fig. 4). As this case shows, caution should be exercised in associating the visualizations with vorticity tagging, particularly when only the still image is given. Caution on this score is also recommended in articles by Hama,[10] Freymuth,[11] and Kurosaka and Sundaram,[12] among others.

Similar structures have been obtained through computation. Orlandi and Verzicco[17] simulated the dye movement in their computation of the vortex ring to compare their simulation with the dye visualization experiment. Advances in recent computational power have begun to allow simulation of experimentally visualized flow (e.g., see Refs. 18 and 19); the technique is expected to be used frequently in the future for better interpretation of experiments as well as for better validation of simulations.

Large Nonplanar Deformation and Breakdown of Vortex Structure

In a jet issuing from a square orifice,[7] four counter-rotating vortices were generated from each corner of the orifice. The cross-sectional contour deformed into a diamond shape and measurements indicated a mixing process faster than that observed in a round jet. Furthermore, the presence of tabs led to a dramatic increase in spreading rate of the jets issuing from various shapes of nozzles.[20] Lasheras et al.[21] imposed periodical radial displacement of azimuthal vorticity on a jet by using a corrugated nozzle and noted counter-rotating streamwise vortices that interacted with vortex rings. Vortex loops formed in alignment with the corrugations and became pinched off downstream. Very recently, Miller et al.[22] reported the results of detailed numerical simulations of circular and three-dimensional jets. The noncircular orifices included square and triangular geometries. The simulation, based on the Navier–Stokes equations, depicted downstream evolution of large-scale vortex structures resulting in streamwise counter-rotating vortices and axis switching. Similar three-dimensional enhancement of mixing is expected in the wake presently studied.

Behind the triangular plate, the large hairpin vortices elongated downstream, and counter-rotating streamwise vortices were observed emanating from the corners (Fig. 4). They are likely to be responsible for the early breakdown of the wake structure. Behind the square plate, the individual arched vortex structures became detached from the vertices of the plate and formed a continuous but highly nonplanar vortex before the organized wake structure was lost. In the wakes behind hexagonal, and octagonal plates, the longitudinal vortices were not explicitly visualized in the experiment, but the out-of-plane deformation of vortex rings and tail formations reflected nonuniform circumferential vorticity fields. Behind a circular disk, even though the wake was initially axisymmetric, a large streamwise deformation of the vortex ring induced an asymmetric crossflow velocity component before vortex shedding. The results are currently being analyzed. In the present experiment, the point in time when the wake loses its initial structure and forms a completely three-dimensional pattern was correlated with model geometries. As expected, the disk wake took the longest time to become three dimensional, and the triangular plate reached its fully three-dimensional stage in about half that time. The wakes behind other geometries lost their original wake structures at a rate approximately inversely proportional to the number of sides.

Conclusions

The flow visualization study in the starting flow showed convoluted deformations and interactions among vortical structures in the wakes behind triangular, square, hexagonal, and octagonal plates. The longitudinal component of the vorticity caused by the arched vortex structure in the initial wake was responsible for the wake deformation and eventual breakdown of the vortex structure. Vortex deformation was prominent with sharp corners, whereas the wake formation behind the octagonal plates started to resemble that behind a disk. Further investigation of these and similar three-dimensional wake structures may lead to better understanding of the breakdown of nominally axisymmetric wake structures and of the unsteady wake structure behind bluff bodies in a steady flow.

Acknowledgments

A portion of this work was supported in part by the National Science Foundation Research Experiences for Undergraduates (NSF REU) program and the U.S. Naval Air Warfare Center. Elvin Chan participated through an earlier NSF REU program in a preliminary study that led to the present work. The final preparation of the article was carried out during the first author's visit to the Institute of Space and Astronautical Science. The visit was supported by the NSF U.S.–Japan Cooperative Science Program monitored by E. Murdy.

References

[1]Koumoutatsakos, P., "Simulation of the Unsteady Viscous Flow Normal to a Zero Thickness Flat Plate," *Journal of Fluid Mechanics* (submitted for publication); also 47th American Physical Society Annual Meeting of the Division of Fluid Dynamics, Nov. 1994.

[2]Higuchi, H., Lu, F., and Chu, Y.-H., "Computations of Unsteady Two-Dimensional Vortex Motions," AIAA Paper 94-2379, June 1994.

[3]Balligand, H., and Higuchi, H., "Experimental Investigation on the Wake Behind a Solid Circular Disk," Sandia National Labs., Rept. SAND 90-7083, Albuquerque, NM, Dec. 1993.

[4]Higuchi, H., and Balligand, H., "Vortex Structure Behind a Disk Started from Rest," *Physics of Fluids A*, Vol. 4, No. 9, 1992, p. 1873.

[5]Widnall, S. E., Bliss, D. B., and Tsai, C.-Y., "The Instability of Short Waves on a Vortex Ring," *Journal of Fluid Mechanics*, Vol. 66, Pt. 1, 1974, pp. 35–47.

[6]Shariff, K., Verzicco, R., and Orlandi, P., "A Numerical Study of Three-Dimensional Vortex Ring Instabilities: Viscous Corrections and Early Non-Linear Stage," *Journal of Fluid Mechanics*, Vol. 279, Nov. 1994, pp. 351–375.

[7]Quinn, W. R., "Streamwise Evolution of a Square Jet Cross Section," *AIAA Journal*, Vol. 30, No. 12, 1992, pp. 2852–2857.

[8]Freymuth, P., Finaish, F., and Bank, W., "Further Visualization of Combined Wing Tip and Starting Vortex Systems," *AIAA Journal*, Vol. 25, No. 9, 1987, pp. 1153–1159.

[9]Chua, K., "Vortex Simulation of Separated Flows in Two and Three Dimensions," Ph.D. Thesis, Graduate Aeronautical Lab., California Inst. of Technology, Pasadena, CA, 1990.

[10]Hama, F. R., "Streaklines in a Perturbed Shear Flow," *Physics of Fluids*, Vol. 5, No. 6, 1962, pp. 644–650.

[11]Freymuth, P., "Vortices," *Handbook of Flow Visualization*, edited by W.-J. Yang, Hemisphere, 1989.

[12]Kurosaka, M., and Sundaram, P., "Illustrative Examples of Streaklines in Unsteady Vortices: Interpretational Difficulties Revisited," *Physics of Fluids*, Vol. 29, No. 10, 1986, pp. 3474–3477.

[13]Higuchi, H., Anderson, R. W., H., and Zhang, J., "Initial Three-Dimensional Wake Formations Behind Various Polygonal Plates," AIAA Paper 94-2283, June 1994.

[14]Toyoda, K., and Hussain, F., "Dynamics of Noncircular Vortex Rings," *Memoirs of the Hokkaido Institute of Technology*, No. 17, Hokkaido Inst. of Technology, Sapporo, Japan, 1989.

[15]Chorin, A. J., "Evolution of a Turbulent Vortex," *Communications in Mathematical Physics*, Vol. 83, No. 4, 1982, pp. 517–535.

[16]Higuchi, H., Balligand, H., and Strickland, J. H., "Numerical and Experimental Investigations of the Unsteady Axisymmetric Flow over a Disk," *Journal of Fluids and Structures* (to be published).

[17]Orlandi, P., and Verzicco, R., "Vortex Rings Impinging on Walls: Axisymmetric and Three-Dimensional Simulations," *Journal of Fluid Mechanics*, Vol. 256, Sept. 1993, pp. 615–646.

[18]Havener, G., and Yates, L., "Visualizing the Flow with CFI," *Aerospace America*, June 1994, pp. 24–27, 43.

[19]Campell, J. F., Chambers, J. R., and Rumsey, C. L., "Observation of Airplane Flowfields by Natural Condensation Effects," *Journal of Aircraft*, Vol. 26, No. 7, 1989, pp. 593–604.

[20]Zaman, K. B. M. Q., "Effect of 'Delta Tabs' on Mixing and Axis Switching in Jets from Asymmetric Nozzles," AIAA Paper 94-0186, Jan. 1994.

[21]Lasheras, J. C., Lecuona, A., and Rodriguez, P., "Three-Dimensional Vorticity Dynamics in the Near Field of Coflowing Forced Jets," *Vortex Dynamics and Vortex Methods*, edited by C. R. Anderson and C. Greengard, Lectures in Applied Mathematics, Vol. 28, American Mathematical Society, Providence, RI, 1991, pp. 403–422.

[22]Miller, R. S., Madnia, C. K., and Givi, P., "Numerical Simulation of Non-Circular Jets," *Computers and Fluids Journal*, Vol. 24, No. 1, 1995, pp. 1–25.